A quantitative approach for analysing bone modelling patterns from craniofacial surfaces in hominins

Natalia Brachetta-Aporta,[1] Paula N. Gonzalez[2] and Valeria Bernal[1] (iD)

[1]*División Antropología, Facultad de Ciencias Naturales y Museo, CONICET, Universidad Nacional de La Plata, La Plata, Argentina*
[2]*CONICET, Unidad Ejecutora-Estudios en Neurociencias y Sistemas Complejos, Florencio Varela, Argentina*

Abstract

Bone size and shape arise throughout ontogeny as a result of the coordinated activity of osteoblasts and osteoclasts, responsible for bone deposition and resorption, and growth displacements. The modelling processes leave specific microstructural features on the bone surface, which can be used to infer the mechanisms shaping craniofacial traits in extinct and extant species. However, the analysis of bone surfaces from fossils and archaeological samples faces some difficulties related to the bone loss caused by taphonomic factors, and the lack of formal methods for estimating missing information and comparing the patterns of bone modelling among several specimens and samples. The present study provides a new approach for the quantitative analysis of bone formation and resorption patterns obtained from craniofacial surfaces. First, interpolation techniques were used to estimate missing data on high-resolution replicas of the left maxilla in a sample of sub-adult and adult modern humans and sub-adult fossil hominins. The performance of this approach was assessed by simulating variable amounts of missing data. Then, we applied measures of dispersion and central tendency to represent the variation and average pattern of bone modelling within samples. The spatial interpolation resulted in reliable estimations of the type of cell activity (deposition or resorption) in the missing areas, even when large extensions of the bone surface were lost. The quantification of the histological data allowed us to integrate the information of different specimens and depict the areas with higher and lower variation in the bone modelling pattern of the maxilla among specimens. Overall, the main advantages of the quantitative approach used here for generating bone modelling patterns are the high replicability and the possibility of incorporating variation among specimens into the comparisons among samples.

Key words: generalized maps; hominin crania; maxilla; missing data; spatial interpolation.

Introduction

The study of microstructural marks left on craniofacial surfaces by the activity of osteoblasts and osteoclasts during the process of bone formation and resorption provides insights into the cellular mechanisms underlying craniofacial variation in extinct and extant species (Mowbray, 2005; Martinez-Maza et al. 2006, 2013, 2016; McCollum, 2008; Kranioti et l. 2009; Lacruz et al. 2013, 2015; Brachetta-Aporta et al. 2014). In particular, the distribution of areas of bone formation and resorption recovered from fossils of immature hominids have been extensively used to compare the bone growth remodelling patterns in facial structures and make inferences about the ontogenetic basis of morphological differences among taxa grounded on general principles of craniofacial growth (Enlow, 1963, 1982; Bromage, 1989; Enlow & Hans, 1996; Martinez-Maza, 2007; McCollum, 2008; Martinez-Maza et al. 2010, 2011, 2013). Taken together, the unique information about ontogenetic processes carried by bone surfaces and the fact that they are analysed by means of non-invasive techniques – which allows the preservation of specimens for future studies – represent the main advantages of the histological analysis of bone surfaces in palaeoanthropological and archaeological research (Boyde, 1972; Bromage, 1984, 1989; Martinez-Maza, 2007; Martinez-Maza et al. 2010). However, the lack of rigorous and formal approaches for the reconstruction of bone surfaces of single specimens with incomplete information and for the assessment of large samples has limited the systematic analysis of fossils and archaeological samples.

The microscopic analysis of osseous surfaces of fossils and bones from archaeological contexts faces some difficulties

related to the natural processes that occur after their deposition. Taphonomic processes such as weathering and erosion alter the bone surface resulting in loss of the marks characteristic of bone formation and resorption, i.e. packs of collagen fibres and concavities known as Howship's lacunae, respectively (Boyde, 1972; Boyde & Jones, 1972; Bromage, 1984). In consequence, the bone modelling patterns obtained from single specimens are invariably fragmentary and heterogeneous (Bromage, 1989). The reconstruction of areas with missing data is thus a necessary first step for any comparative analysis of bone modelling patterns. Despite being a common issue in palaeohistological studies, the procedures for estimating complete maps from incomplete information have not been thoroughly discussed. For single specimens this is usually accomplished by expanding the information from locations where bone formation or resorption can be recorded to those locations where information is lacking, under the assumption that surface bone growth modelling takes place in the form of patches (Bromage, 1989). The type of bone surface assigned to a given location with missing data and the extension of such areas are based on qualitative criteria set by the observer, and are thus hardly reproducible. This not only means that reconstructions made by different observers can differ, but also that the assumptions underlying such differences cannot be assessed (Brachetta-Aporta, 2016). Moreover, the qualitative procedures ignore the uncertainties inherent to any reconstruction process, which need to be taken into account for validating the inferences made on the basis of estimated data (Gunz et al. 2009). Consequently, the development of quantitative approaches is required to provide more objective and replicable estimates of missing data from bone surfaces.

Additionally, the use of qualitative methods has important limitations for making comparisons of bone modelling patterns across several specimens. Such comparisons are usually done between maps of single specimens that are considered as representative of a certain group (e.g. species, sex, age) or between maps (referred as generalized maps) that represent the most frequent pattern of cell activity within those groups (Martinez-Maza et al. 2013, 2016; Lacruz et al. 2015). On one hand, as the maps are visually assessed, the degree of similarity among groups is difficult to estimate. On the other hand, neither the use of individual nor generalized maps takes into account the within-group variation (McCollum, 2008). The inferences made about the processes that underlie the differences within and between species can thus be biased as a consequence of underestimating the natural variability of the spatial distribution of bone formation and resorption areas.

Here, we propose a new approach for the quantitative analysis of bone formation and resorption patterns obtained from high-resolution replicas of craniofacial surfaces. First, we present a method for estimating missing data in bone modelling maps based on spatial interpolation techniques. By this procedure, complete maps of single specimens can be obtained applying explicit and objective criteria. Then, we use measures of dispersion (range) and central tendency (median) to represent the variation and average pattern of bone modelling maps within a sample of specimens. The performance of the method for the reconstruction of complete maps of single specimens was first assessed by simulating variable amounts of missing information in three maxillae of modern *Homo sapiens*. We then applied this method to an archaeological sample of modern adult and sub-adult humans from Argentina (Gonzalez et al. 2010), and a sample of fossils from Sima de Los Huesos (Spain; Lacruz et al. 2015). Finally, on the basis of interpolated maps we estimated generalized maps for each sample.

Materials and methods

Samples

We analysed a total of 13 specimens including modern humans and fossils (Table 1). Ten specimens correspond to modern humans from prehistoric aboriginal groups of South America. These remains were found in archaeological sites located in North-western Argentina (Pampa Grande, Salta province) and are housed in the División Antropología of Museo de La Plata, Argentina (González, 1972; Baldini et al. 2003). These individuals were selected taking into consideration a set of variables that macroscopically describe the degree of surface alteration: post-deposition bone loss; fragmentation; post-deposition fractures; weathering stage; presence of carbonate, manganese and copper oxide and root marks; rodent and carnivore marks and modern man-made marks (Behrensmeyer, 1978; Buikstra & Ubelaker, 1994; Lyman, 1994). Only individuals with good preservation were sampled in order to maximize the histological information recovered (Martinez-Maza et al. 2006). Also, individuals displaying alveolar remodelling due to abscesses, ante mortem tooth loss and high degree of wear, among others factors, were excluded (Buikstra & Ubelaker, 1994).

The age of death of the archaeological specimens was estimated by means of dental and osteological criteria. The obliteration of the sphenobasilar suture was first used to separate sub-adults from adults. Then, the sequence of tooth formation and eruption was analysed to estimate the age of sub-adults (Buikstra & Ubelaker, 1994; AlQahtani et al. 2010), while the age of adults was estimated by the degree of obliteration of ectocranial sutures of the antero-lateral region (Meindl & Lovejoy, 1985). We also calculate the percentage of cells with histological information in each high-resolution cast (Table 1).

Additionally, we analysed three sub-adults from Sima de Los Huesos (SH hominins; Lacruz et al. 2015). The information about the age of death of these specimens and the type of microscope used for the observation of histological data was obtained from Lacruz et al. (2015) and is shown in Table 1. The percentage of information available is not provided for the fossils because the original maps are not shown in the paper by Lacruz et al. (2015).

Histological analysis

High-resolution casts of the surface of the left maxilla were obtained and analysed under the microscope for the identification

Table 1 Summary of samples used. Crosses indicate which specimens were included in each analysis.

Specimen	Estimated age (years)	Microscopy	Missing data estimation	Generalized maps	Cells with histological data (%)
Modern human					
Sub-adult					
17769	6.5	ILM		x	92.98
17783	6.5	ILM	x	x	96.67
17774	8	ILM		x	93.33
17780	8	ILM		x	98.43
17787	14	ILM	x	x	97.33
Adult					
17688	35–45 (Female)	ILM		x	41.07
17726	35–45 (Female)	ILM		x	33.19
17744	35–45 (Female)	ILM	x	x	86.93
17690	35–45 (Male)	ILM		x	59.43
17724	35–45 (Male)	ILM		x	88.89
SH fossil*					
Cranium 9	~ 12	Confocal		x	–
AT 1100	16–18	SEM		X	–
AT 5899	Late adolescent	SEM		X	–

ILM, incident light microscope; SEM, scanning electron microscope. The percentage in the last column was estimated as the number of cells with histological information relative to the total number of cells in the digital grid.
*Specimens from Sima de los Huesos (SH) in Lacruz et al. (2015).

of bone modelling fields (Fig. 1). Briefly, the procedure involves: cleaning the bone surface by applying 60% alcohol with a brush with soft and fine bristles; obtaining a negative cast of the surface with a low-viscosity silicon (Coltene President light body); producing a positive cast with epoxy resin (Tolken), which is then covered by a thin layer of gold-palladium (for more details about the procedure used, see Brachetta-Aporta et al. 2014; Fig. 2A,B).

To guide the systematic observation under the microscope, cells of 5 × 5 mm were drawn on the metallized surface of each cast (Fig. 2B). The presence of bone formation and resorption activity was observed using an optical microscope Olympus CX31 (20 × NA 0.40 objective) with incident light and recorded in bone modelling maps. After the observation of each cast, the maps were scanned and converted to digital images (Fig. 2C).

In order to make the bone modelling maps comparable (generating homologized maps), we performed least-squares generalized Procrustes and thin-plate spline deformation analyses. Briefly, the

procedure involves: (i) digitizing eight points of reference (landmarks) on each image (except in the case of fossils in which the infraorbital foramen was not visible, so only seven points were digitized; Fig. 2D) – the reference points were chosen according to two criteria, they are evenly placed along the contour of the maps and allow a good description of their main features; (ii) performing a generalized Procrustes superimposition in order to centre, scale and rotate the configurations of landmarks; (iii) obtaining a consensus configuration on which each individual map was then deformed or warped (Fig. 2E); (iv) warping the image of each specimen using the thin-plate spline deformation so the landmarks correspond with their position in the consensus configuration (Fig. 2F). These procedures were performed in tpsDig2 v2.17 and tpsSuper v2.03 (Rohlf, 2015). Then, a digital grid was placed on the warped images using ImageJ 1.49v (Fig. 2D,E; Abràmoff et al. 2004). The number of cells of this digital grid was set to maximize the chances of having only one type of activity (formation or resorption) in each cell: 93 for
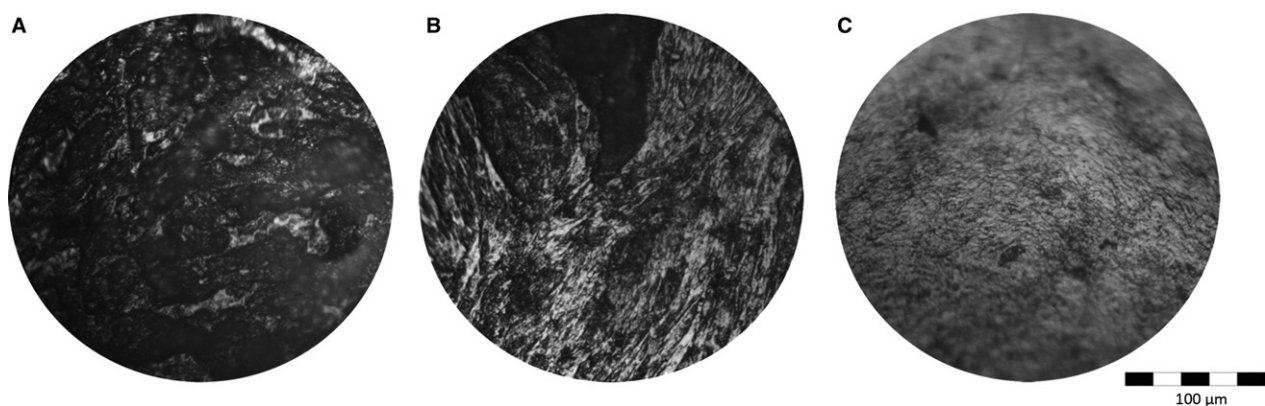

Fig. 1 Bone modelling surface identified. (A) Bone resorption, (B) bone formation and (C) no histological data.
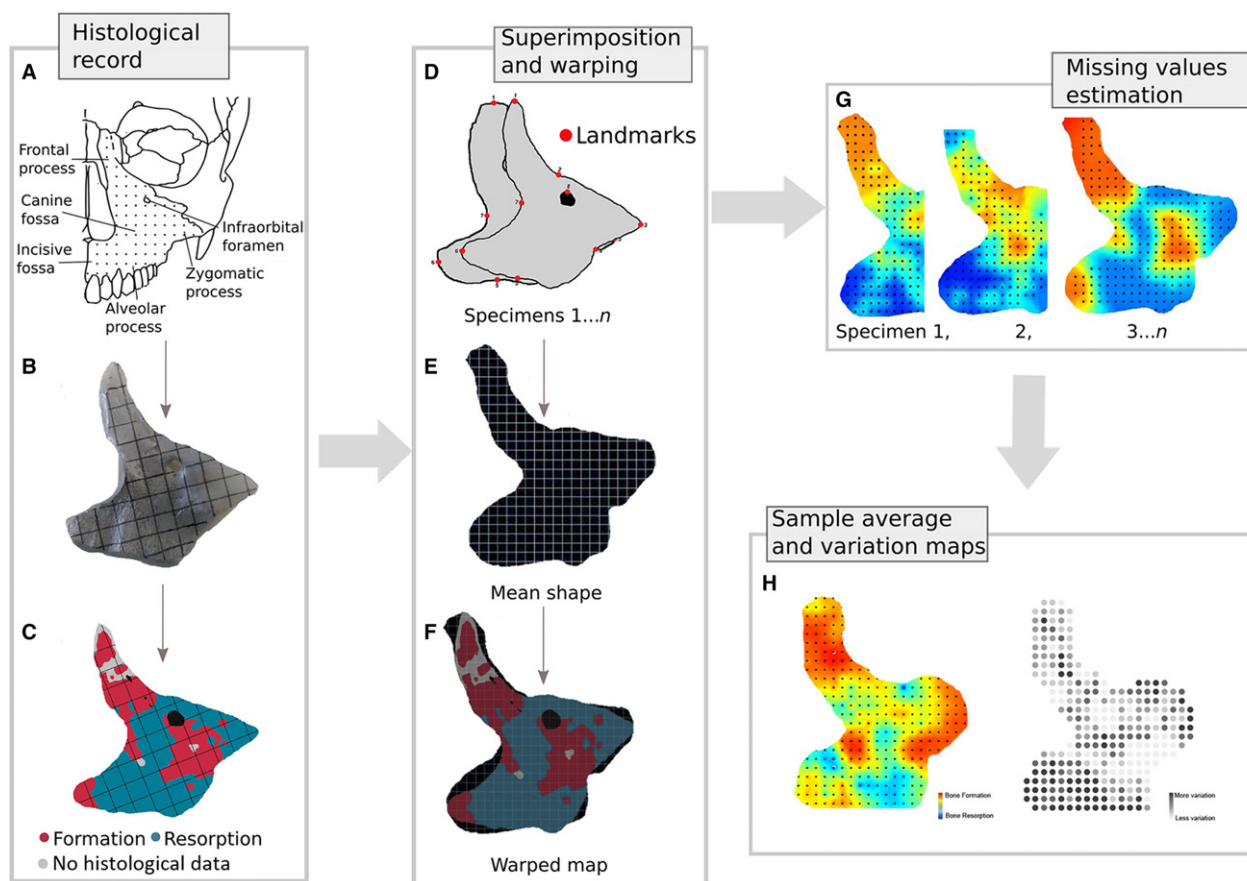
Fig. 2 Schematic representation of the steps for the acquisition and quantitative analysis of bone modelling maps. (A) Regions of the maxilla analysed; (B) coated cast with the grid used for observation under the microscope; (C) digital grid; (D–F) steps for the estimation of the average shape and warping; (G) interpolation for estimating missing data in each individual map; (H) maps used to represent the median and range values within a sample. Landmarks in (D) 1: extreme of the frontal process; 2: intersection between the orbital border and the zygomaxillary suture; 3: extreme of the zygomatic process; 4: point between the alveolar and zygomatic processes; 5: point in the middle of the alveolar process; 6: point located between nasion and prostion; 7: alar; 8: point placed at the superior border of the infraorbital foramen.

modern adults; 268 for modern sub-adults; and 220 for SH hominins. In particular, a greater number of cells was used for the sub-adults because these specimens displayed larger extensions of surface with histological information, and the areas of bone resorption and formation were alternated and spatially contiguous. In such a case, larger cells will likely include more than one type of bone activity but only the most represented will be recorded. This could result in an important loss of information of the smaller patches. The information contained in each cell was registered as follows: −1 = presence of bone resorption (Fig. 1A); 1 = presence of bone formation (Fig. 1B); 0 = presence of both types of bone activity, and empty when no information was available (this could represent either bone loss by taphonomic processes or resting surfaces; Fig. 1C). Cells were numbered in both axes (x, y) starting on the inferior left square (coordinates: 1,1; Martinez-Maza, 2007).

Exploring the spatial structure of bone modelling maps

We evaluated the spatial structure of the bone modelling maps by means of spatial correlograms (Legendre & Fortín, 1989; Barbujani, 2000). In particular, we explored the distribution of values of bone

formation and resorption in the cells across the map to determine whether they follow a random distribution or, alternatively, closer cells tend to display values more similar than expected by chance. The statistic used in the correlograms was the Moran's I coefficient, which describes the spatial autocorrelation among cells in the space. This coefficient is computed summing the covariation between sampling units at a given distance apart (i.e. distance class) and then the sum is divided by the number of pairs of sampling units in that distance class. Moran's I coefficient is related to Pearson's correlation, and takes values between −1 and +1. Positive values for a distance class indicate that cells at that distance tend to be similar, while negative values indicate that they tend to differ. Here, the Moran's I coefficient was calculated for 15 distance classes. This number of distance classes was estimated on the basis of the Sturge's rule (Legendre & Legendre, 1998), which determines the number of histogram classes on the basis of sample size. The number of classes D is computed by this formula:

$$D = 1 + 3.3 \times \log 10 \, n(n^2 - 1),$$

where n is the sample size and in this case corresponds to the number of cells in the grids. Finally, spatial

correlograms were generated by plotting the Moran's I coefficients against the distance classes.

The spatial correlograms of the bone modelling maps showed a positive autocorrelation at short distances, which means that neighbour cells tend to display the same type of cell activity (Fig. 3). As the distance among cells increases, their values of cell activity tend to differ.

Because closer cells tend to display the same type of cell activity, the spatial pattern of bone modelling can be described using the linear interpolation method based on the inverse distance weighting (IDW) criteria. In this method, the data missing in a given location are estimated using the known values in a restricted neighbourhood search area. The underlying assumption is that nearby locations likely have similar values. Hence, the missing values are estimated as a weighted average of the known values from nearby points. Particularly, the values are weighted in inverse proportion to the distance, i.e. the square root of the distance, between points. The formula of the IDW interpolation can be expressed as:

$$\hat{Z}(x_0) = \frac{\sum\limits_{j=1}^{m} z(x_j) d_{ij}^{-k}}{\sum\limits_{j=1}^{m} d_{ij}^{-k}},$$

where $\hat{Z}(x_0)$ is the value of the variable z at the missing locations, $z(x_j)$ is the value of the variable at the sampled location j, m is the number of neighbour locations, d_{ij} is the distance between the unsampled location i and sampled location j, and the exponent k is a real value from 0 to 1. The advantage of this linear interpolation is that it better preserves the local spatial patterns, which is especially relevant when the distribution is heterogeneous as is the case in bone modelling patterns. The spatial interpolation was run in Past 3.02a (Hammer et al. 2001).

Estimation of missing data by spatial interpolation

The interpolation method was then used to estimate missing data by replacing the empty cells by the interpolated values. Here, the interpolation of missing values of each map was done on the homologized maps so the data obtained within a sample are comparable. Note that the same procedure can be applied to the original maps when only single specimens are analysed. We tested the reliability of these estimations in a sub-sample of three specimens (Tables 1 and 2) by randomly removing information from a variable number of cells. The elimination of cells for these simulations was at random given that all areas in a bone surface are expected to have equal chances of being affected by processes that erode the marks of bone modelling activity. In particular, we randomly removed the information of 25, 50, 75 and 90% of total cells in each map. Then, the missing information was replaced by the values obtained from the spatial interpolation using the available data in each map. For each specimen, the value obtained for each cell in the simulations (columns 3–6 in Fig. 4) was compared with the interpolated values obtained using all the information available (IDW column in Fig. 4). As the value given to the cells in each case corresponds to a repeated measurement of the same object, it is possible to evaluate the concordance between data derived from interpolating missing information and the complete dataset (Müller & Büttner, 1994). We calculated the intraclass correlation coefficient (ICC), which estimates the proportion of the total variation that is due to the variation between cells and provides a reference of the degree of agreement between estimations (Fleiss, 1981; Müller & Büttner, 1994). The analysis was made in R 3.1.1, with psy package (R Development Core Team, 2014).

Construction of generalized maps

Maps representing the bone modelling pattern of each sample (sub-adult and adult modern humans, and sub-adult SH fossils) were estimated on the basis of the interpolated values of each cell in the individual maps. First, we calculated the median value of each cell within the three samples and represented these values on colour maps. Here, the median was used because this measure of central tendency is more robust to the effect of outliers, which is particularly important for small sample sizes as is usually the case for fossil and archaeological remains. Second, the range of values for each cell within each of the three samples was calculated and represented on a map to provide a measure of among-individual variation. The interpolated maps for each specimen were obtained in Past 3.02a using the procedure described in previous paragraphs. The maps displaying the range value for each cell were made in R 3.1.1, with maptools, RColorBrewer and classInt packages (R Development Core Team, 2014).

Results

Estimation of missing data by spatial interpolation

The missing data estimated by spatial interpolation for the two sub-adults and the adult specimen of modern humans are shown by colour maps in Fig. 4. Each colour map shows the distribution of bone formation and resorption on the maxillary surface, calculated on the basis of the available information at variable percentages of cells randomly removed.

The interpolated map obtained with the full available information for one of the adult specimens (17744) shows bone formation in the frontal process, around the infraorbital foramen, and between the posterior region of the body of the maxilla and the lower region of the zygomatic process (Fig. 4). Bone resorption, on the other hand, is predominant along the alveolar process, in the region of the incisive and canine fossae, and in the upper region of the zygomatic process. Also, resorption activity is observed in the lower region of the frontal process. This pattern of distribution persisted when the interpolation was made after removing information from 25 and 50% of the cells. The pattern changes slightly when 75% of the data was removed. While the frontal process and the incisive fossa still display the presence of bone formation and resorption, respectively, the preponderance of formation activity in the surrounding area of the infraorbital foramen, the posterior region of the body of the maxilla and zygomatic process is not preserved. The distribution of the bone resorption throughout the canine fossa remains. By contrast, the
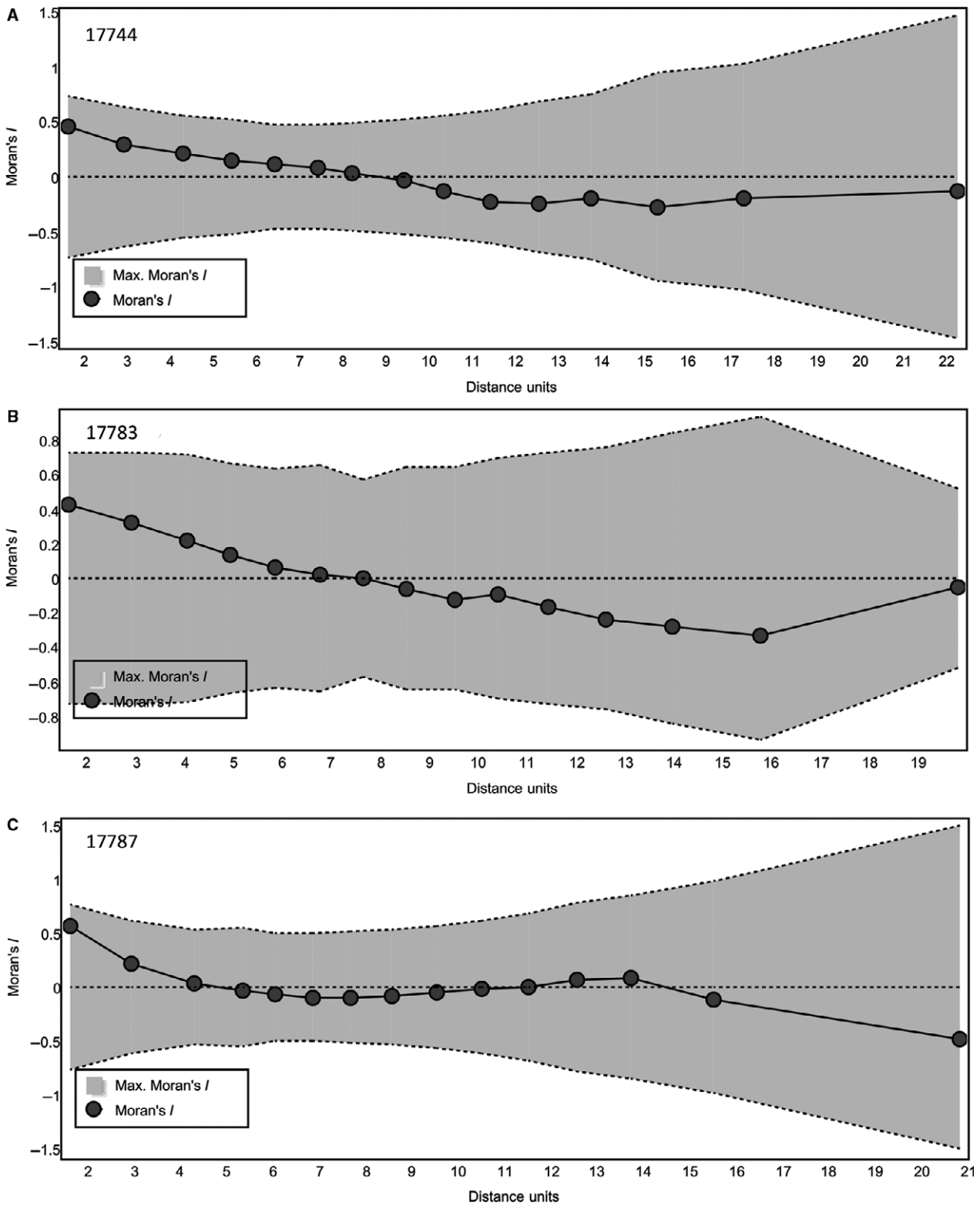
Fig. 3 Spatial correlograms. The horizontal axis represents the distance classes, and the vertical axis displays the Moran's I coefficients estimated for each distance class.

Table 2 ICCs between interpolations obtained with all the information originally available and with variable percentages of information randomly removed.

	Percentage of information removed			
Specimen	25%	50%	75%	90%
17774	0.97	0.94	0.83	0.64
17783	0.94	0.87	0.79	0.73
17787	0.99	0.96	0.85	0.64

distribution of bone modelling activities presents some changes when the interpolation is done after subtracting 90% of the data. The frontal process no longer exhibits predominance of bone formation, and areas of bone resorption are observed in the upper region. The zygomatic process only shows bone formation, while the information of bone resorption is not preserved. The alveolar process and the incisive fossa preserve the presence of bone resorption, but the canine fossa and the posterior region of the body of the maxilla present a more uniform distribution of both modelling activities.

The bone modelling pattern obtained from the total cells with information for the sub-adult specimen 17783 shows the presence of formation between the lower region of the

frontal process, the canine fossa and the zygomatic process (Fig. 4). This distribution is crossed by patches of bone resorption, particularly in the zygomatic process. A predominance of bone resorption is seen at the upper part of the frontal process and the alveolar process, and around the canine fossa. This pattern is similar to that obtained after removing 25% of cells, only a patch of formation activity in the area adjacent to the nasal notch is lost. When the interpolation is done on the basis of 50% of the cells, bone formation surfaces are observed along the lower region of the frontal and zygomatic processes, maintaining a patch with bone resorption near the infraorbital foramen. Areas of bone resorption are predominantly found in the upper region of the frontal process and the area of the incisive fossa, and along the alveolar process. The distribution of bone resorption decreases along the upper part of the body of the maxilla and is virtually absent in the zygomatic process. A similar pattern is preserved for 75% of the cells, although bone formation is not as preponderant as in the previous maps and the distribution of bone resorption patches increases along the frontal process. The patch of bone resorption near to the infraorbital foramen is also lost. This pattern is further modified when 90% of the cells are missing. In this case the map is characterized by a continuous distribution of both types of cell activity, with the presence of bone formation in the base of the frontal process
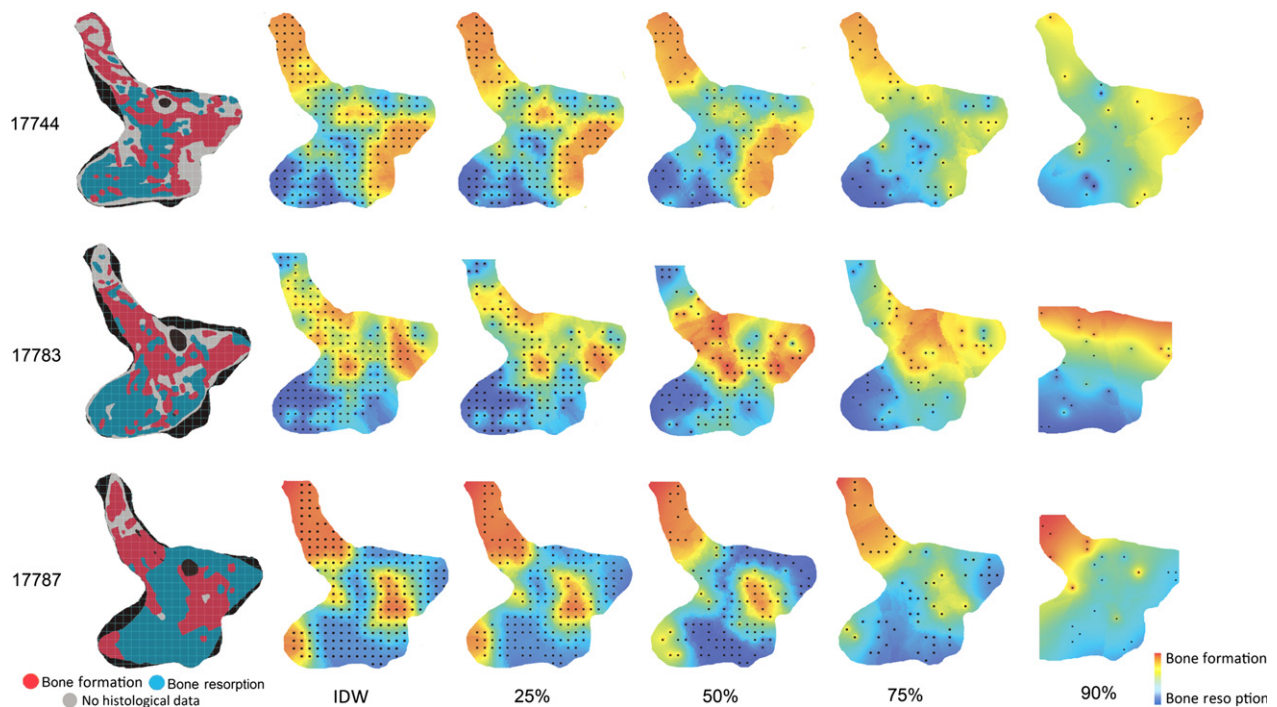

Fig. 4 Bone modelling maps of two sub-adults and one adult of the modern human sample. The first column represents each individual map warped onto the mean shape (bone formation in red, resorption in blue, and absence information in white). The second column represents the colour maps obtained from interpolated data using the total of cells available. The rest of the columns show the colour maps obtained from interpolated data using variable percentages of missing cells. Dots on these maps represent the centre of each cell of the grid (comprised by 273 cells) represented in the first column.

and the upper ridge of the zygomatic process, while the alveolar process is characterized by bone resorption. Note that the last colour map no longer represents the full shape of the maxilla; the areas corresponding to the upper frontal process, the extreme of the zygomatic process and the incisive fossa are missing. This is related to the non-homogeneous distribution of information when only 10% of the data is available.

The last sub-adult analysed (17787) presents predominance of bone formation in the frontal process, the intersection between the canine fossa and zygomatic process and the incisive fossa (Fig. 4). Bone formation activity is also observed in the area behind the nasal notch. Conversely, areas of bone resorption are observed along the alveolar and zygomatic processes, the canine fossa and the lower region of the frontal process. This pattern remains when 25 and 50% of the cells are removed, although in the second case the predominance of bone formation in the incisive fossa decreases. When 75% of the data is removed, the pattern tends to be similar. Conversely, when 90% of the data is subtracted, the distribution of areas of cell activity changes, showing bone formation only in the lower region of the frontal process. As in the previous map, the upper frontal process, the extreme of the zygomatic process and the area of the incisive fossa are missing due to the non-homogeneous sampling with so few cells.

The ICC values indicate that the estimation of missing data by the interpolation method presents an 'excellent' agreement compared with the original values when information of 25, 50 and even 75% of the cells are removed (Table 2). However, the degree of agreement decreases when 90% of the cells are removed (Table 2). These results are consistent with the qualitative assessment of the maps described in the previous paragraphs.

Construction of generalized maps

Figures 5–7 show the median bone modelling maps (a) and the range value maps (b) for sub-adult and adult modern humans, and the SH fossils. The shape of these maps represents the consensus image of the maxillae of each sample. The common bone modelling map of each sample represents the median values calculated on the basis of interpolated data of each individual map, while the range value maps show the among-individual variation in the values of each cell within samples. In the later, darker colours represent most variable cells among individual maps.

Sub-adult modern humans

The information represented in the median map clearly distinguishes three areas according to the predominant type of bone activity (Fig. 5A). The frontal process is characterized by the predominance of bone formation, the alveolar process and the area surrounding the incisive fossa display predominance of bone resorption, while in the region of the zygomatic process and the canine fossa both activities are observed. Even though this last area mostly presents resorption, there is a patch of bone formation around the infraorbital foramen. This last area also presents the highest values for the range (Fig. 5B). Other cells that also show high range values are the extreme of the frontal process and the incisive fossa. Although formation predominates on the frontal process, it is not exclusive (Fig. 5B). On the other hand, the incisive fossa presents resorption on four of five maps.

Adult modern humans

The map of median values displays predominance of bone formation over resorption (Fig. 6A). The frontal and zygomatic processes, and the area behind the nasal notch are characterized by bone formation. Formation surfaces, although in a lesser extent, are also found in the anterior portion of the alveolar process, the incisive fossa and the area surrounding the canine fossa. Conversely, the posterior portion of the alveolar process, the canine fossa and the region above the nasal notch mostly display bone resorption. A patch of bone resorption is also found over the infraorbital foramen. The predominance of bone formation
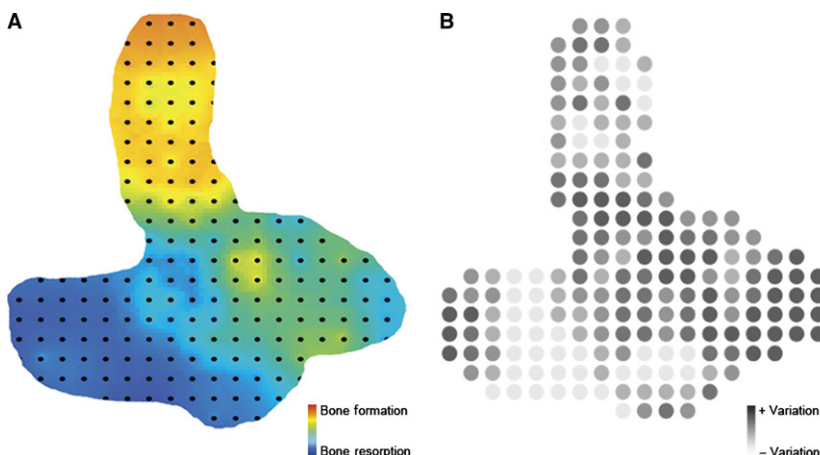

Bone formation
Bone resorption

+ Variation
– Variation

Fig. 5 (A) Median bone modelling map and (B) range value map of maxillary bone obtained for the five modern human sub-adults. Dots represent the centre of each of the 193 cells used for this sample.

Fig. 6 (A) Median bone modelling map and (B) range value map of maxillary bone obtained for the five adults. Dots represent the centre of each of the 268 cells used for this sample.
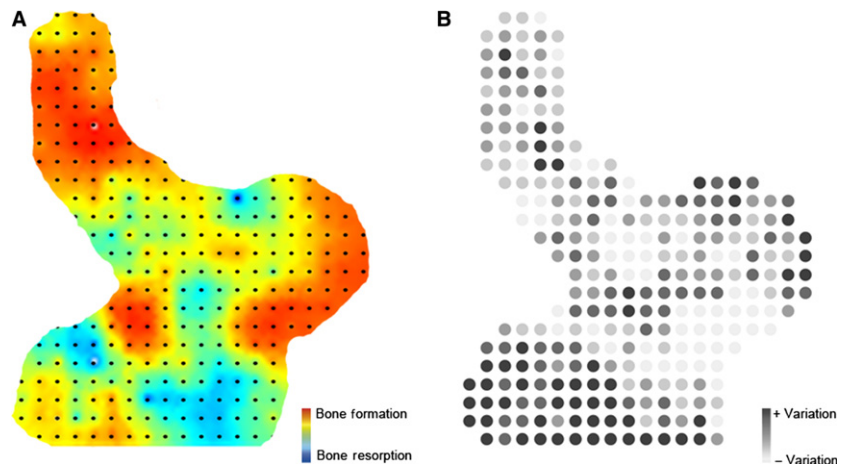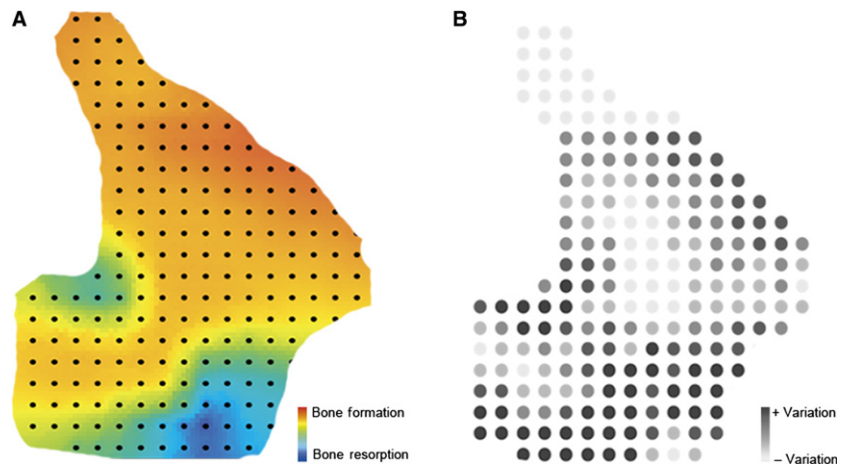

Fig. 7 (A) Median bone modelling map and (B) range value map of maxillary bone obtained for the three SH fossils. Dots represent the centre of each of the 210 cells used for this sample.

in the frontal process and in the inferior edge of the zygomatic process, and the presence of both activities between them is the most constant pattern. Instead, the rest of the maxilla shows high range values of activity (Fig. 6B).

SH fossils

The map of median values shows predominance of bone formation, except in the posterior portion of the alveolar process where there is bone resorption. Above the nasal notch there is predominance of resorption activity (Fig. 7A). The alveolar process and the area over the nasal notch show high range values, while the frontal process and the area of the canine fossa area display more constant values across specimens (Fig. 7B).

Discussion

In this study we provided a quantitative approach for the reconstruction and analysis of bone modelling maps obtained from high-resolution replicas of craniofacial surfaces. This approach comprises the estimation of missing histological data of individual bone structures and the computation of generalized maps that represent the modelling patterns in groups of individuals. We showed that the distribution of formation and resorption areas exhibits a strong spatial structure, meaning that closer cells tend to display the same type of bone activity, while they tend to differ as the distance among them increases. Given such spatial structure of formation and resorption areas, the interpolation based on the IDW resulted in an appropriate criterion for estimating the type of surface in areas with missing data. The spatial interpolation based on this criterion allowed reliable estimations even when up to 75% of the cells were randomly lost. This means that good estimations of bone modelling patterns could be obtained with as little as 25% of the cells exhibiting information about bone activity, while estimations based on lesser amounts of data should be taken with caution. This is relevant because bone surfaces with scarce histological information are the usual case due to both the limitations of some microscopic techniques for obtaining data on large areas [e.g. scanning electron microscopy (SEM), confocal; Martinez-Maza et al. 2010; Lacruz et al. 2015] and the effect of taphonomic processes (Bromage, 1984; Lacruz et al. 2015). Overall, the

interpolation technique applied here is highly replicable and, thus, the process for filling the areas with missing data is less affected by intra- and inter-observer error.

We also showed that the accuracy of the reconstructions not only depends on the amount but also on the structure of missing data. The simulations run in this study were based on randomly missing data. In some cases, the cells without information were grouped together in specific areas leading to the loss of data of an entire anatomical region. Such regions cannot be interpolated by the IDW criterion because it relies on data available from neighbour areas. The same issue is faced when the missing areas are filled by the observer according to qualitative criteria. Consequently, the estimation of missing values in areas for which no information is available is still challenging and other alternatives need to be explored. An option could be filling those areas on the basis of common maps as those obtained here, although large samples should be first analysed to evaluate the effect of inter-individual variation on those estimations.

A common issue in the study of archaeological and palaeontological bones is how to interpret areas characterized by smooth and polished surfaces that are compatible either with formation or resorption (Martinez-Maza, 2007). Such bone surfaces can represent the effect of taphonomic processes such as abrasion (Bromage, 1984) or being areas without bone formation or resorption activity, with mineralizing front advances (i.e. resting surfaces, Boyde, 1972). The limitations for differentiating both types of surfaces lead us to consider them as missing data, with the consequent chance of overestimating the extension of formation and resorption areas in the interpolated maps. Bone integrity gradually reduces as a consequence of the loss of collagen and the action of taphonomic processes after individual death (Knüsel & Robb, 2016). Consequently, the overestimation of missing data can have a greater impact in fossils and archaeological remains than in modern samples. To discuss the effect of taphonomy on the loss of bone surface, we evaluated the association between the weathering stage (Behrensmeyer, 1978) of each bone and the percentage of surface that exhibited information about the type of cell activity (Appendix S1). We did not find a consistent association between both variables, bones with high degrees of weathering exhibit lower percentages of missing data than bones with lower weathering stages. In consequence, the greater percentage of information recovered in sub-adults compared with adults could reflect biological rather than taphonomic processes. Unlike sub-adults, the adult skeleton is maintained by removing and replacing a fraction of it each year (Marks & Odgren, 2002). Accordingly, Boyde (1972) recognized long periods of quiescence in adults, while in fetal individuals bone activity extends across the entire surface. This is in agreement with several studies that only report fields of deposition and resorption on the bone surface of sub-adult maxilla (McCollum, 2001,

2008; Martinez-Maza, 2007; Martinez-Maza et al. 2013). Consequently, it is more likely that areas without signs of bone activity correspond to resting surfaces in adults compared with sub-adults.

Once complete maps of single specimens are obtained, the next step in any comparative analysis is to assess the similarities and differences of the bone modelling patterns among groups. On the basis of the interpolated maps of each specimen, we obtained maps that represent the median values and the range of variation of bone activity in the three samples under study, i.e. modern human sub-adults and adults, and sub-adult SH fossils. For modern humans some differences in the median maps of sub-adults and adults were observed, mainly related to the larger extension of areas of bone resorption in the alveolar and zygomatic processes among sub-adults. Comparisons with previous studies are difficult to perform given that most of them report specific ages for young individuals (Kurihara et al. 1980; Enlow, 1982; McCollum, 2001; Martinez-Maza, 2007), and data for adults are almost lacking (see Martinez-Maza, 2007 for an exception). The median map obtained for the modern human sub-adults is in general similar to the generalized patterns previously reported (Enlow, 1982; Martinez-Maza, 2007; Martinez-Maza et al. 2013). However, these studies describe a consistent presence of resorption in the canine fossa and zygomatic process, while in our sample those areas displayed high ranges of variation. This is in agreement with the high levels of variation in the distribution of formation and resorption surfaces in the facial region recognized for the age range studied here (Kurihara et al. 1980; Martinez-Maza, 2007; McCollum, 2008).

With regard to modern human adults, the median map obtained here is similar to that reported for a sample of young adults of European origin (Martinez-Maza, 2007). Despite the differences in the age profile between both samples, a general concordance is observed, particularly along the frontal process and the canine fossa, which is characterized by bone formation. In contrast, some discrepancies are found around the nasal notch and in the inferior zygomatic process. In particular, this last area exhibited bone formation instead of resorption as previously reported (Enlow, 1982; Martinez-Maza, 2007; Martinez-Maza et al. 2013). Even though low levels of variation have been suggested for adults (Martinez-Maza, 2007), our analyses reveal that some areas of zygomatic and alveolar processes can be highly variable. Such contrasts could be attributed to differences in ancestry as most studies are based on samples of recent populations of European origin. Additionally, the effect of environmental factors, especially food hardness related to the items consumed and food-processing techniques cannot be discarded. The analysis of more prehistoric samples is necessary to thoroughly discuss the causes of the differences in the bone modelling patterns among populations.

Finally, the range map of the SH specimens clearly differentiates areas with more consistent values across specimens from highly variable areas. Most variation was restricted to the alveolar process, while the frontal process and the canine fossa exhibited lower levels of variation among individuals. Overall, our results remark the importance of assessing how well the generalized maps represent a given sample, considering the inter-individual variation. In this sense, the map displaying the range of variation for each cell can be used to set apart highly variable areas from those that display a more consistent pattern of bone activity across the sample.

In summary, the quantitative approach applied here for generating bone modelling maps allowed us to overcome some of the limitations of the qualitative analysis. First, the reconstruction of individual maps by using explicit and rigorous criteria for estimating missing data increases the replicability of the analysis and allows the assessment of the accuracy of the reconstructions obtained. Second, generalized maps calculated on the basis of complete interpolated maps provide a more accurate representation of a given sample than the maps obtained using only the distribution of activity actually observed. If individual bones exhibit large areas of missing data, the latter procedure will tend to represent the few specimens in which bone formation and resorption areas were registered. The quantification of bone modelling maps also has the advantage of explicitly incorporating individual variation into the analyses. Finally, the acquisition of complete maps from fragmentary data opens up the opportunity of performing multivariate analyses and combining the palaeohistological information in structural and functional studies, which will contribute to discuss the factors that underlie the craniofacial variation in hominins.

Acknowledgements

Funding

Author contributions

NBA: design, acquisition of data, data analysis, drafting of the manuscript; PNG: design, data analysis, interpretation, critical revision of the manuscript; VB: design, data analysis, interpretation, drafting of the manuscript.

References

Abràmoff MD, Magelhaes PJ, Ram SJ (2004) Image processing with ImageJ. *Biophotonics Int* **1**, 36–42.

AlQahtani SJ, Hector MP, Liversidge HM (2010) The London atlas of human tooth development and eruption. *Am J Phys Anthropol* **142**, 481–490.

Baldini MI, Baffi EI, Salaberry MT, et al. (2003) Candelaria: una aproximación desde un conjunto de sitios localizados entre los cerros de las Pirguas y el Alto del Rodeo (Dto. Guachipas, Salta, Argentina). In: *La Mitad Verde del Mundo Andino*. (eds Ortiz G, Ventura B), pp. 131–152. Jujuy: EDIUNJU.

Barbujani G (2000) Geographic patterns: how to identify them and why. *Hum Biol* **72**, 133–153.

Behrensmeyer AK (1978) Taphonomic and ecologic information from bone weathering. *Paleobiology* **4**, 150–162.

Boyde A (1972) Scanning electron microscope studies of bone. In: *The Biochemistry and Physiology of Bone*. (ed. Bourne GH), pp. 259–310. New York, NY: Academic Press.

Boyde A, Jones SJ (1972) Scanning electron microscope studies of bone. In: *The Biochemistry and Physiology of Bone*, 2nd edn. (ed. Bourne GH), pp. 259–310. New York, NY: Academic Press.

Brachetta-Aporta N (2016) Error intraobservador en el análisis paleohistológico de superficies craneofaciales. *Rev Arg Antrop Biol* **18**(2), 1–11.

Brachetta-Aporta N, Martinez-Maza C, Gonzalez P, et al. (2014) Bone modeling patterns and morphometric craniofacial variation in individuals from two prehistoric human populations from Argentina. *Anat Rec* **297**, 1829–1838.

Bromage TG (1984) Surface remodelling studies on fossil bone. *J Dent Res* **63**, 491.

Bromage TG (1989) Ontogeny of the early human face. *J Hum Evol* **18**, 751–773.

Buikstra J, Ubelaker D (1994) *Standards for Data Collection from Human Skeletal Remains*. Fayetteville: Arkansas Archaeological Survey.

R Development Core Team (2014) *R: a Language and Environment for Statistical Computing*. Vienna: R Foundation for Statistical Computing.

Enlow DH (1963) *Principles of Bone Remodelling*. Springfield, IL: Thomas CC Publisher.

Enlow DH (1982) *Handbook of Facial Growth*. Philadelphia, PA: W.B. Saunders.

Enlow DH, Hans MG (1996) *Essentials of Facial Growth*. Philadelphia, PA: W.B. Saunders.

Fleiss JL (1981) *Statistical Methods for Rates and Proportions*. New York, NY: Wiley.

González AR (1972) Descubrimiento arqueológico en la Serranía de Las Pirguas. *Pcia de Salta* **24**, 388–392.

Gonzalez PN, Perez SI, Bernal V (2010) Ontogeny of robusticity of craniofacial traits in modern humans: a study of South American populations. *Am J Phys Anthropol* **142**, 367–379.

Gunz P, Mitteroecker P, Neubauer S, et al. (2009) Principles for the virtual reconstruction of hominin crania. *J Hum Evol* **57**, 48–62.

Hammer Ø, Harper DAT, Ryan PD (2001) PAST: paleontological statistics software package for education and data analysis. *Palaeontol Electronica* **4**, 1–9.

Knüsel CJ, Robb J (2016) Funerary taphonomy: an overview of goals and methods. *J Archaeol Sci* **10**, 655–673.

Kranioti EF, Rosas A, García-Vargas S, et al. (2009) Remodeling patterns of occipital growth: a preliminary report. *Anat Rec* **292**, 1764–1770.

Kurihara S, Enlow DH, Rangel RD (1980) Remodeling reversals in anterior parts of the human mandible and maxilla. *Angle Orthod* **50**, 98–106.

Lacruz RS, Bermúdez de Castro JM, Martinón-Torres M, et al. (2013) Facial morphogenesis of the earliest Europeans. *PLoS One* **8**, e65199.

Lacruz RS, Bromage TG, O'Higgins P, et al. (2015) Ontogeny of the maxilla in Neanderthals and their ancestors. *Nat Commun* **6**, 8996.

Legendre P, Fortín MJ (1989) Spatial pattern and ecological analysis. *Vegetatio* **80**, 107–138.

Legendre P, Legendre L (1998) *Numerical Ecology*. Amsterdam: Elsevier.

Lyman RL (1994) *Vertebrate Taphonomy*. Cambridge: Cambridge University Press.

Marks SC, Odgren PR (2002) Structure and development of skeleton. In: *Principles of Bone Biology*. (eds Bilezikian JP, Raisz LG, Rodan GA), pp. 3–15. California: Academic Press.

Martinez-Maza C (2007) *Ontogenia y Filogenia del Modelado Óseo en el Esqueleto Facial y la Mandíbula de los Hominoideos. Estudio de la Línea Filogenética Neandertal a Partir de las Muestras de Atapuerca-SH y El Sidrón*. Madrid: Tesis de Doctorado, Facultad de Ciencias Biológicas, Universidad Complutense de Madrid.

Martinez-Maza C, Rosas A, García-Vargas S (2006) Bone paleohistology and human evolution. *J Anthropol Sci* **84**, 33–52.

Martinez-Maza C, Rosas A, Nieto-Diaz M (2010) Identification of bone formation and resorption surfaces by reflected light microscopy. *Am J Phys Anthropol* **143**, 313–320.

Martinez-Maza C, Rosas A, Garcia-Vargas S, et al. (2011) Bone remodelling in Neanderthal mandibles from the El Sidrón site (Asturias, Spain). *Biol Lett* **7**, 593–596.

Martinez-Maza C, Rosas A, Nieto-Diaz M (2013) Postnatal changes in the growth dynamics of the human face revealed from the bone modelling patterns. *J Anat* **223**, 228–241.

Martinez-Maza C, Freidline SE, Strauss A, et al. (2016) Bone growth dynamics of the facial skeleton and mandible in *Gorilla gorilla* and *Pan troglodytes*. *Evol Biol* **43**, 63–80.

McCollum MA (2001) Variation in the growth and modeling of the human maxilla as revealed by scanning electron microscopy. *Scanning* **23**, 71.

McCollum MA (2008) Nasomaxillary remodeling and facial form in robust *Australopithecus*: a reassessment. *J Hum Evol* **54**, 2–14.

Meindl RS, Lovejoy CO (1985) Ectocranial suture closure: a revised method for the determination of skeletal age at death based on the lateral-anterior sutures. *Am J Phys Anthropol* **68**, 57–66.

Mowbray K (2005) Surface bone histology of the occipital bone in humans and chimpanzees. *Anat Rec* **283B**, 14–22.

Müller R, Büttner P (1994) A critical discussion of Intraclass Correlation Coefficients. *Stat Med* **13**, 2465–2476.

Rohlf FJ (2015) The tps series of software. *Hystrix* **26**, 9–12.

Supporting Information

Additional Supporting Information may be found in the online version of this article:

Appendix S1. Weathering stages of bone surfaces.